Watermarking for Multimedia Security Using Complex Wavelets

Alastair I. Thompson
Queen's University, Belfast, UK
Email: athompson13@qub.ac.uk

Ahmed Bouridane
Northumbria University, Newcastle, UK, King Saud University, Riyadh, Saudi Arabia
Email: Ahmed.Bouridane@unn.ac.uk, A.Bouridane.c@ksu.edu.sa

Fatih Kurugollu
Queen's University, Belfast, UK
Email: f.kurugollu@qub.ac.uk

Camel Tanougast
LICM-ISEA, Université Paul Verlaire, Metz, France
Email: Camel.Tanougast@univ-metz.fr

Abstract—**This paper investigates the application of complex wavelet transforms to the field of digital data hiding. Complex wavelets offer improved directional selectivity and shift invariance over their discretely sampled counterparts allowing for better adaptation of watermark distortions to the host media. Two methods of deriving visual models for the watermarking system are adapted to the complex wavelet transforms and their performances are compared. To produce improved capacity a spread transform embedding algorithm is devised, this combines the robustness of spread spectrum methods with the high capacity of quantization based methods. Using established information theoretic methods, limits of watermark capacity are derived that demonstrate the superiority of complex wavelets over discretely sampled wavelets. Finally results for the algorithm against commonly used attacks demonstrate its robustness and the improved performance offered by complex wavelet transforms.**

Index Terms—**Complex wavelets, spread transform, capacity, human visual system, watermarking.**

I. Introduction

DIGITAL data hiding has gained popularity in recent years as a way of settling intellectual property rights disputes, the ease with which digital media can be perfectly duplicated and distributed has led to a need for a method of identifying the original owner of the image.

Data hiding allows for the embedding of information in a host signal that can later be extracted as proof of ownership or for some other purpose. This information directly into the host media so that it can not be removed without applying significant distortion to the host. Robustness, imperceptibility and capacity are the three conflicting attributes of data hiding systems. This paper aims to achieve new standards of imperceptibility by adapting and comparing two main methods of deriving visual models for watermarking to the complex wavelet transforms. One is derived from the wavelet coefficients using visual tests and the other from an adaptation of a universal spatial JND (just noticeable distortion) profile.

It is proposed that higher levels of capacity and robustness can be achieved through the use of spread transform data hiding. Spread transform was devised with the aim of combining the two main methods of data hiding, Spread Spectrum (SS) and Quantization Index Modulation (QIM) [2]. It also incorporates dual tree wavelets that lead to improved imperceptibility over discretely sampled wavelets.

Recently there has been a move towards a theoretical analysis of the maximum achievable performance of watermarking schemes. To address this, Moulin et al. [11, 12] have developed an information theoretic model that models the watermarking situation as a game between the attacker and embedder with each trying to maximize their advantage over a range of Gaussian distributed channels.

In this paper the capacity of several different embedding domains and images are derived by modeling the considered wavelet decompositions as a series of parallel Gaussian channels. Using an established statistical model per-channel capacities are

derived for the case of spread transform watermarking [16-17]. The optimal attack and embedding strategies are derived through the use of a game theoretic approach.

Manuscript received February 8, 2010. This work was supported in part by a grant from the European Social Fund (ESF).

doi:10.4304/jmm.5.5.443-457

Finally empirical results for a range of common attacks such as gaussian noise, compression and filtering are given for a range of different images and embedding conditions.

II. EMBEDDING DOMAIN

An important consideration is the domain in which the watermarking will take place. Early watermarking algorithms used the spatial domain [13]. However these algorithms showed poor robustness, for this reason watermarking moved to the transform domain. Some transform domains used include the DFT (discrete fourier transform) and DCT (discrete cosine transform). Although these were an improvement over the spatial domain they have been replaced in recent years by the wavelet domain. The wavelet domain provides a much better approximation of the HVS (human visual system) and possesses better energy compaction properties.

A. Discrete Wavelet Transform

The DWT consists of filtering the source image with both a high pass (detail) and low pass (coarse) filter, and then down-sampling then result. The process is then repeated in the other direction for both the coarse and detail sub-band to create 4 sub-bands - the low pass sub-band and the horizontal, vertical and diagonal detail sub-bands. The wavelet filter used in the proposed algorithm is the biorthogonal 9/7 tap filter as used in the JPEG2000 compression algorithm.

The disadvantage of the DWT is its inability to differentiate between opposing diagonal features as shown in figure 1 with both being represented in the same diagonal sub-band.

Figure 1. Note how the caption is centered in the column.

B. Dual Tree Complex Wavelet Transform

The DT DWT uses two DWTs acting in parallel on the same data. It is the real version of the dual tree complex wavelet transform (DT CWT) [8]. One DWT acts upon the even samples of the data while the other acts upon the odd. The difference and sum of these two DWT decomposition are then taken to produce the two trees of the DTWT (figure 3).

Although the complex version has the advantage of excellent shift invariance this comes at the cost of 4:1 redundancy for 2-D signals which places restrictions upon the embedding algorithm as watermark in the wavelet domain must have a valid representation in the spatial domain. For this reason it was decided to use the real version developed by Selesnick instead which has a much more manageable redundancy of 2:1 (figure 2) for 2-D signals allowing for more freedom when embedding [15].

The DTWT overcomes the problem of the DWT lacking directional selectivity. The DTWT can discriminate between opposing diagonals with six different sub-bands orientated at 15°, 75°, 45°, -15°, -75° and -45° (figure 4). This also allows better representation of vertical and horizontal features.

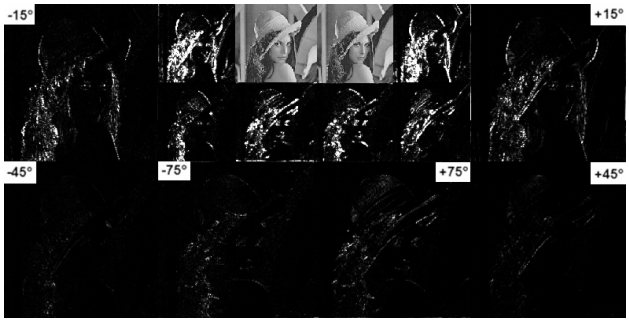

Figure 2. DTWT Decomposition

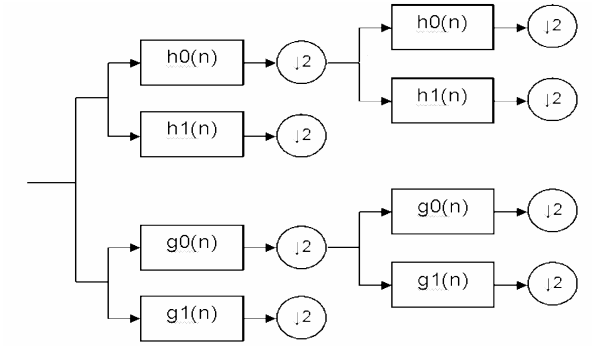

Figure 3. DTWT Filterbank

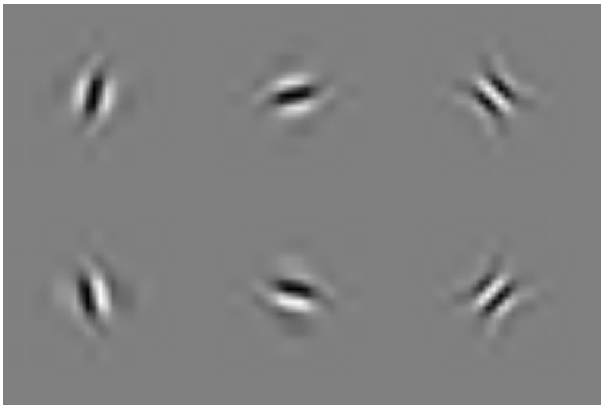

Figure 4. DTWT Filterbank

B. Non Redundant Complex Wavelet

The non redundant complex wavelet transform has been developed by Fernandes et al. [5] as an alternative to the class of over complete, redundant complex wavelet transforms. It makes use of a tri-band filterbank where the data is down-sampled by 3 at each stage.

There are two filterbanks NRWT and NCWT defined that are applied to real and complex inputs respectively. In the case of the NRWT the output consists of one real

part and two complex outputs. These two complex outputs are conjugates of each other and so one can be disregarded (figure 6). In the case of the NCWT the output consists of 3 complex outputs.

The sub-bands produced are orientated at 0°, 90°, 45° and -45°, both real and imaginary (figure 7). While offering less directional sub-bands than the DTCWT the NRCWT is able to discriminate between opposing diagonals with no increase in redundancy.

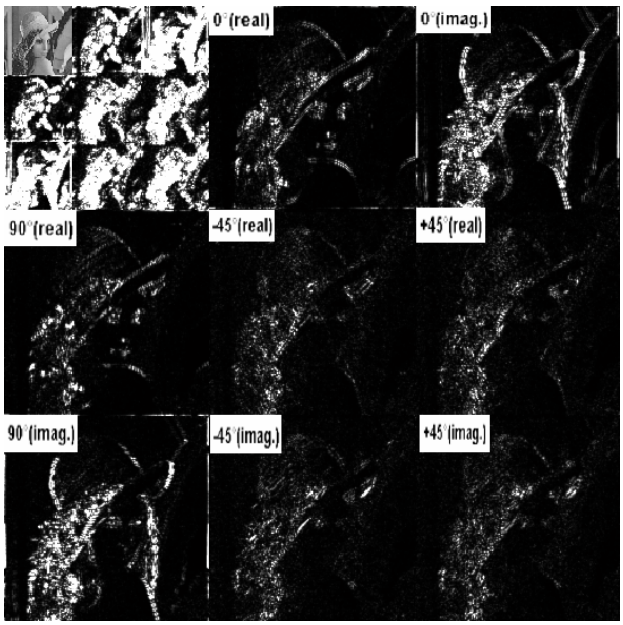

Figure 5. NRCWT Decomposition

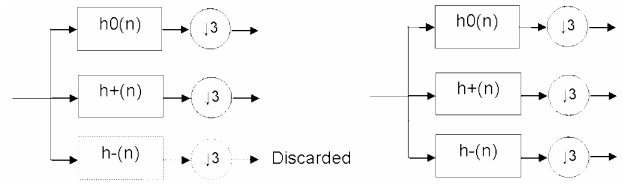

Figure 6. NRCWT Filterbank for real and complex inputs respectively

Figure 7. NRCWT Coefficients

III. VISUAL MODEL

To satisfy the imperceptibility requirement it is necessary to limit the distortion applied to each individual coefficient of the wavelet decomposition. For this purpose a JND profile for each individual coefficient must be derived. Two main factors can be identified as contributing the masking effect of the human visual system, these are:

Luminance Masking: Distortions in bright and very dark areas of the image are less visible than those in areas of the image with middling brightness.

Spatial Masking: Textured areas and edges in an image are much better at masking distortions than smoother areas where the spatial variation is much smaller.

Two methods of deriving the JND model are adapted for use in the algorithm. One that directly uses the wavelet coefficients and a series of visual test, and another that adapts a spatial JND profile to fit the sub-band structure.

A. Loo's Method

A series of visual tests were conducted to obtain the JND value for each of the individual coefficients down to the 5th level of decomposition. The algorithm was applied using both the DWT and DT DWT domains so tests were conducted for both. Loo [9] proposed a JND model calculated as shown in equation 3.1.

$$g_{l,\theta}(u,v) = B\sqrt{k^2 x_{l,\theta}^2 + C_{l,\theta}^2} \qquad (1)$$

Where k and C are sub-band dependent constants, dependent on the level l and orientation θ. The value x is the absolute mean value of a 3x3 gaussian window of standard deviation 0.5 centred round the coefficient at position (x,y). B is a measure of the spatial brightness corresponding to the coefficient at position (u,v).

$$B = 2.12(y(u,v) - 0.56)^2 + 1 \qquad (2)$$

$$B = 2.03(y(u,v) - 0.53)^2 + 1 \qquad (3)$$

$$B = 2.43(y(u,v) - 0.55)^2 + 1 \qquad (4)$$

Where y represents the value of the level 5 low-pass coefficient corresponding to position (u,v). The visual tests were conducted by setting all sub-bands of an image to 0. Then all the values in the sub-band under consideration were set randomly distributed in the range $[0,n]$. The image was then recomposed and added to a sine wave grating of the appropriate frequency and orientation. The value n was then increased uniformly until the distortion became visible. Using the value of n and the average value of the coefficients composing the sine wave grating, an estimate of k for each level and orientation was derived. The tests were repeated with different amplitudes of sine wave gratings to obtain varied results for multiple values of x. The results for both the DWT, DTWT and NRCWT are shown in table 1.

TABLE I. LOO'S JND FACTORS

Sub-band	DWT-k	DWT-C	DTDWT-k	DTDWT-C	NRCWT-k	NRCWT-C
Level 1 – Diag.	0.33	5	1.00	6	0.25	3
Level 1 – Hor./Ver.	0.20	3	0.60	4.5	0.16	2
Level 2 – Diag.	0.25	4	0.50	1.5	0.15	2
Level 2 – Hor./Ver.	0.14	2	0.25	1	0.145	1
Level 3 – Diag.	0.25	1	0.25	1	0.145	1
Level 3 – Hor./Ver.	0.11	1	0.21	1	0.14	1
Level 4 – Diag.	0.18	1	0.20	1	-	-
Level 4 – Hor./Ver.	0.11	1	0.195	1	-	-
Level 5 – Diag.	0.18	1	0.195	1	-	-
Level 5 – Hor./Ver.	0.11	1	0.19	1	-	-

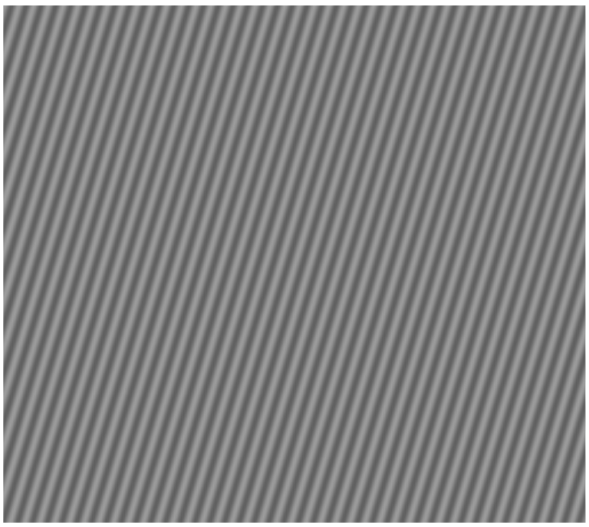

Figure 8. Sine wave grating

All visual tests were conducted with a gamma correction value of 2.1, a resolution of 32 pixels/cm and a viewing distance of 30 cm.

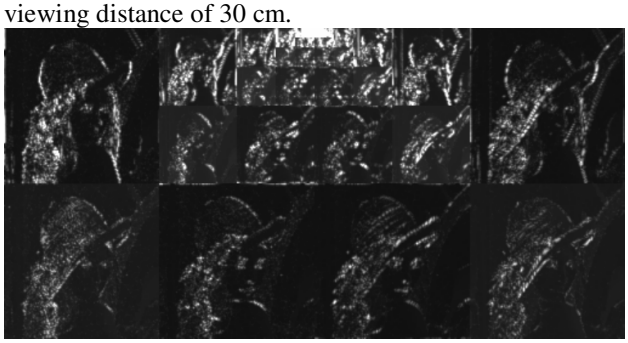

Figure 9. Loo's JND decomposition for DTWT

B. Chou's Method

Chou's method [3] operates by composing a full-band JND model in the spatial domain and then decomposing it into separate sub-band JND profiles. Similar to Loo's method the JND values are modeled as the dominant effects of both overall luminance and luminance contrast. The full-band JND model is contructed from the following equations:

$$JND_{fb}(x,y) = \max\{f_1(b_g(x,y), m_g(x,y)), f_2(b_g(x,y))\} \quad (5)$$

$$f_1(b_g(x,y), m_g(x,y)) = m_g(x,y)\alpha(b_g(x,y)) + \beta(b_g(x,y)) \quad (6)$$

$$f_2(b_g(x,y)) = T_0 \cdot \left(1 - \left(\frac{b_g(x,y)}{127}\right)^{1/2}\right) + 3; \quad \text{for } b_g(x,y) \le 127$$

$$f_2(b_g(x,y) - 127) + 3; \quad \text{for } b_g(x,y) > 127 \quad (7)$$

Through visual experiments Chou derived T_0, γ and λ were found to be 17, 3/128 and ½ respectively. The values $b_g(x,y)$ and $m_g(x,y)$ are the average background luminance and luminance contrast around the pixel at (x,y) respectively. They are obtained using the following filters:

$$G_1 = \begin{bmatrix} 0 & 0 & 0 & 0 & 0 \\ 1 & 3 & 8 & 3 & 1 \\ 0 & 0 & 0 & 0 & 0 \\ -1 & -3 & -8 & -3 & -1 \\ 0 & 0 & 0 & 0 & 0 \end{bmatrix} \quad G_2 = \begin{bmatrix} 0 & 0 & 1 & 0 & 0 \\ 0 & 8 & 3 & 0 & 0 \\ 1 & 3 & 0 & -3 & -1 \\ 0 & 0 & -3 & -8 & 0 \\ 0 & 0 & -1 & 0 & 0 \end{bmatrix}$$

$$G_3 = \begin{bmatrix} 0 & 0 & 1 & 0 & 0 \\ 0 & 0 & 3 & 8 & 0 \\ -1 & -3 & 0 & 3 & 1 \\ 0 & -8 & -3 & 0 & 0 \\ 0 & 0 & -1 & 0 & 0 \end{bmatrix} \quad G_4 = \begin{bmatrix} 0 & 1 & 0 & -1 & 0 \\ 0 & 3 & 0 & -3 & 0 \\ 0 & 8 & 0 & -8 & 0 \\ 0 & 3 & 0 & -3 & 0 \\ 0 & 1 & 0 & -1 & 0 \end{bmatrix}$$

$$m_g(x,y) = \max_{k=1,2,3,4}\{|grad_k(x,y)|\} \quad (10)$$

$$|grad_k(x,y)| = \frac{1}{16}\sum_{i=1}^{5}\sum_{j=1}^{5} p(x-3+i, y-3+j).G_k(i,j) \quad (11)$$

And for average background luminance:

$$B(i,j)=\begin{bmatrix}1&1&1&1&1\\1&2&2&2&1\\1&2&0&2&1\\1&2&2&2&1\\1&1&1&1&1\end{bmatrix}$$

$$b_g(x,y)=\frac{1}{32}\sum_{i=1}^{5}\sum_{j=1}^{5}p(x-3+i,y-3+j).B(i,j) \quad (12)$$

Finally, the individual sub-band JND profiles are calculated as for a multi-resolution decomposition as follows:

$$JND_q^2(x,y)=\left[\sum_{i=0}^{2^t-1}\sum_{j=0}^{2^t-1}JND_{fb}^2(i+x.2^t,j+y.2^t)\right].\omega_q \quad (13)$$

for q = 0,1,…,15 and 0 <= x <= N/2^t, 0 <= y <= N/2^t

and $\begin{cases} t=5-\left\lfloor\frac{p-1}{3}\right\rfloor, & if \quad 0<p\le 15 \\ t=5, & if \quad p=0 \end{cases}$

$JND_q(x,y)$ represents the JND value at position (x,y) of the qth sub-band. The factor ω_k is calculated as follows:

$$\omega_q=\left(S_q.\sum_{k=0}^{15}S_k^{-1}\right)^{-1} \quad (14)$$

Where p is the number of sub-bands used in the decomposition. S_k denotes the average sensitivity of the HVS to distortions in the kth sub-band. It is calculated as:

$$S_k=\frac{16}{N.N}\sum_{u=\varepsilon_k.h}^{(\varepsilon_k+1)h-1}\sum_{v=p_k.w}^{(p_k+1)w-1}\varepsilon(u,v) \text{ for k = 0,1,….,15} \quad (15)$$

$\varepsilon(u,v)$ denotes the response curve of the modulation transfer function or MTF for 0<=u<=N, 0<=v<=N. Chou proposes the following formula for its calculation:

$$\varepsilon(u,v)=a.\left[b+\left(\frac{\Omega(u,v)}{\Omega_0}\right)\right].\exp\left[-\left(\frac{\Omega(u,v)}{\Omega_0}\right)^c\right] \quad (16)$$

where

$$\Omega(u,v)=\left[\left(\frac{32v}{N}\right)^2+\left(\frac{24u}{N}\right)^2\right]^{1/2} \quad (17)$$

Fig 3.4 is derived from the MTF curve modeled by a=2.6, b=0.0192, c=1.1 and Ω_0=8.772.

The model as originally proposed by Chou has a linear sub-band structure that is not suitable for the decomposition structure of the discrete and complex wavelet transforms. For this reason a different sub-band structure is proposed for the DTWT (figure 10). Each section of the dual tree decomposition is treated as being of the same channel sub-band. For the DWT only the right hand side is used.

The same sub-band weight is applied to opposing halves of the dual tree composition as they are of the same orientation and frequency and so can be treated identically in this respect. In addition, to take into account the improved directionality of the DTWT a different set of filters are used to obtain the value of m with G1 and G2 orientated at -15 and + 15 degrees respectively and G5 and G6 orientated at -75 and +75 degrees respectively.

$$G_1=\begin{bmatrix}0&0&-1&0&0\\-1&-3&-3&0&0\\0&0&0&0&0\\0&0&3&3&1\\0&0&1&0&0\end{bmatrix}\quad G_2=\begin{bmatrix}0&0&-1&0&0\\0&0&-3&-3&-1\\0&0&0&0&0\\1&1&3&0&0\\0&0&1&0&0\end{bmatrix}$$

$$G_3=\begin{bmatrix}0&0&1&0&0\\0&8&3&0&0\\1&3&0&-3&-1\\0&0&-3&-8&0\\0&0&-1&0&0\end{bmatrix}\quad G_4=\begin{bmatrix}0&0&1&0&0\\0&0&3&8&0\\-1&-3&0&3&1\\0&-8&-3&0&0\\0&0&-1&0&0\end{bmatrix}$$

$$G_5=\begin{bmatrix}0&0&0&1&0\\0&0&0&3&0\\-1&-3&0&3&1\\0&-3&0&0&0\\0&-1&0&0&0\end{bmatrix}\quad G_6=\begin{bmatrix}0&-1&0&0&0\\0&-3&0&0&0\\-1&-3&0&3&1\\0&0&0&3&0\\0&0&0&1&0\end{bmatrix}$$

m is then calculated using equation (18)

$$m_g(x,y)=\max_{k=1,2,3,4,5,6}\{|grad_k(x,y)|\} \quad (18)$$

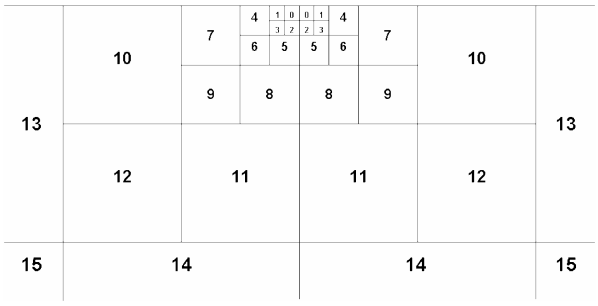

Figure 10. DTWT decomposition for Chou's Model

As the NRCWT down-samples by three at each level and has only 4 sub-bands at each level the decreased number of sub-bands must be taken into account. Imaginary and real parts of each sub-band are considered

as being in the same channel leading to four different channels at each level for a total of 13 channels. Equation (13) is then altered to take into account the reduction in the number of channels in the sub-band decomposition and the down-sampling by 3 instead of 2 at each level

$$JND_q^2(x,y) = \left[\sum_{i=0}^{3^t-1} \sum_{j=0}^{3^t-1} JND_{fb}^2(i + x.3^t, j + y.3^t) \right] .\omega_q \tag{19}$$

for q = 0,1,…,12 and 0 <= x <= $N/3^t$, 0 <= y <= $N/3^t$

$$\text{and} \quad \begin{cases} t = 3 - \left\lfloor \frac{p-1}{4} \right\rfloor, & if \quad 0 < p \le 12 \\ t = 3, & if \quad p = 0 \end{cases}$$

The calculation of the factor ω_q is also calculated to take into account the reduction in channels from 15 to 12.

$$\omega_q = \left(S_q . \sum_{k=0}^{12} S_k^{-1} \right)^{-1} \tag{20}$$

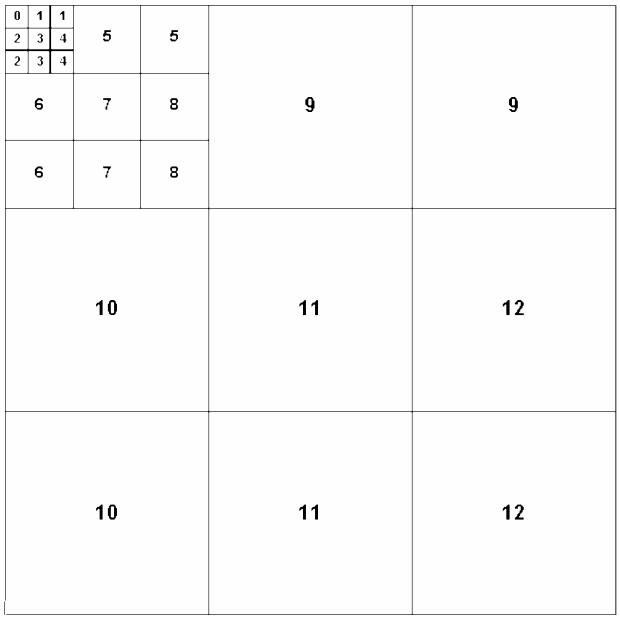

Figure 11. NRCWT decomposition for Chou's Model

As can be seen in figure 12 the JND model accurately scales JND vales according to edges in the image as well as adjusting watermark strength according to background luminance. When compared with figure 9 it can be seen that Chou's model is much more effective at adapting the JND values to edges. Another significant advantage of Chou's model over Loo's is that it can be applied to any wavelet transform without having to do an independent set of visual tests.

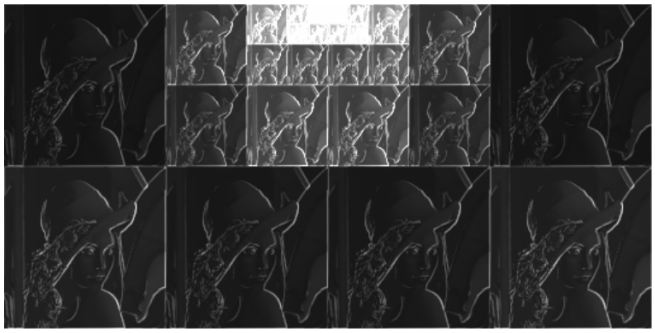

Figure 12. Chou's JND decomposition for DTWT

IV. Spread Transform Embedding

Spread transform data hiding was originally proposed by Chen and Wornell [2] as an extension of quantization index modulation (QIM) where data is quantized using a scalar quantizer Δ to carry data. It applies QIM in a lower dimensional space across several samples in an effort to combine the advantages of QIM and spread spectrum methods. Quantization is applied to vectors composed of host samples rather than individual host samples.

$$x^{ST} = \sum_{n=1}^{r} x_n v_n \tag{21}$$

Where x^{ST} represents host samples, v a key dependent vector and r the length of the vector used.

$$x^{ST} = q(x^{ST}; \Delta/\alpha) + (1-\alpha)[x^{ST} - q(x^{ST}; \Delta/\alpha)] \tag{22}$$

Where Δ is the quantization step used and α is a distortion compensation factor that ranges in value from 0 to 1. The optimum value of α will vary according to the watermark-noise ratio (WNR), with higher levels of α being optimum for higher levels of WNR.

A. Proposed Algorithm

The proposed algorithm proceeds as follows:

1. A binary pseudo-random key *K* of the same size as the host image is generated (an optional dither can be added for increased security).

2. The image is decomposed to 5 levels using either discrete or complex wavelet transforms.

3. The JND values for each individual coefficient in the decomposition is calculated using either Loo's method or Chou's method.

4. Coefficients are selected from subbands to carry individual watermark bits.

5. The quantization step Δ is calculated based upon the JND values of the coefficients to ensure that embedding does not exceed the perceptual limit.

6. The current value of the vector projection is calculated by multiplication of the host coefficients with the key values corresponding to the host coefficients.

7. Individual host coefficients are then scaled appropriately so the vector projection corresponds to quantization bin equal to the bit to be embedded. Each individual coefficient is scaled by the size of its corresponding jnd value. This jnd value is multiplied by the vector quantization step divided by the sum of all jnd values corresponding to the vector to be quantized to ensure the correct final value of the vector projection. Finally it is multiplied by the corresponding value in the key dependent vector which will be either 1 or -1.

8. The wavelet sub-bands are then recomposed to give the watermarked image.

B. Information Theoretic Analysis

Letting the watermark MSE be equal to D_1, the attacker distortion equal to D_2 and the watermark to noise ratio (WNR) equal to $10log_{10}(D_1/D_2)$, Eggers and Girod [4] show that the effective gain in WNR over QIM when using spread transform is equal to:

$$WNR_r = WNR_1 + 10\log_{10} r \tag{23}$$

and that the capacity C of spread transform data hiding can be calculated from the capacity of embedding without spread transform (r=1) as follows:

$$C_{ST,r}^{AWGN} = \frac{C_{ST,1}^{AWGN}(WNR + 10\log_{10} r)}{r} \tag{24}$$

Approximations are provided for the optimum spread factor r and distortion compensation value α in what they call the spread transform scalar costa scheme (ST-SCS) which is the algorithm used for embedding in this paper. (23) can be solved using (24)

$$C_{ST,1}^{AWGN} = \max_{\alpha} I(y;d) \tag{25}$$

where y is the data received by the decoder, d is equal to 0 or 1 for binary data embedding and I is the mutual information. (24) is solved through a comparison of the PDFs of the transmitted and received data. Finally the power of the watermark distortion is given by (26).

$$E\{q^2\} = \frac{\Delta^2}{12} \tag{26}$$

The advantage of spread transform is its complete independent of interference from the host image. It also offers capacities that are generally higher than spread spectrum for low to moderate levels of attack.

1) Parallel Gaussian Channels

To derive capacity limits it is necessary to divide the source image into separate channels. To divide the wavelet coefficients of an image into separate channels the model proposed by Lopresto et al. [10] has been used. Within this scheme wavelet sub-bands are modeled as Gaussian distributions with zero mean and variance dependent upon the coefficient's location within the wavelet sub-bands to create independent parallel channels. The coefficients' variances lie in a quantization band k where $1 \le k \le K$. The channels are designated as follows:

1. Apply 5 levels of DWT or DTCWT. Due to the greater down-sampling by 3 at each level of the NRCWT only 3 levels of decomposition are used.

2. Calculate the local variance in a 5x5 window for finer detail levels (1,2,3) and 3x3 window for coarser levels (4,5). For the NRCWT the 5x5 window is applied to levels 1&2 while the 3x3 window is applied to level 3.

3. The natural logarithm of each variance is quantized using K levels and step size Δ. A channel then consists of all coefficients with the same quantized variance within every sub-band.

The quantizer step size Δ is determined by the range of variances in the sub-band decomposition.

In this work, K equal to 256 is used. The estimated 256 parallel Gaussian channels are shown in figure 13 for the DTWT decomposition of the 'Lena' image, where black = channel 1, white = channel 256.

Simpler images like 'Lena' will tend to have lower rates for higher power channels, while textured images like 'Baboon' will tend to have high power channels with high rates.

Each channel is assumed to be i.i.d and Gaussian with zero mean and variance σ_k^2. Each channel has an inverse sub-sampling rate R_k. For all transforms channels are critically sampled so that:

$$\sum_{k=1}^{K} R_k = 1 \tag{27}$$

2) Watermarking Game

The problem of finding the capacity can be viewed as a game across the parallel gaussian channels [11,12] where both embedder and attacker attempt to maximize their advantage in every channel. For the capacity estimates to be meaningful distortion constraints are imposed upon both the embedder and the attacker. For the channel model under consideration the embedder and attacker distortions are given as:

$$\sum_{k=1}^{K} r_k \theta_k e_k = D_1 \tag{28}$$

$$\sum_{k=1}^{K} r_k \theta_k a_k = D_2 \tag{29}$$

where θ is the distortion modifier for the channel j dependent upon the orientation and level of the coefficients in the channel, e and a are the weighted MSE of the attack and embedding strategy respectively.

The three distortions placed upon embedder and attacker are:

$$0 \le e_k \tag{30}$$

$$e_k \le a_k \tag{31}$$

$$a_k \le p_k \tag{32}$$

where p_k is the original power of the channel k. The capacity of the parallel Gaussian channels is then given by the maximization-minimization relation shown in (33).

$$C = \max_{e_k} \min_{a_k} \sum_{k=1}^{K} r_k \Gamma(p_k, e_k, a_k) \tag{33}$$

The solution to (33) for SAWGN attacks is given in the following sub-section:

The SAWGN attack involves both the addition of AWGN noise and amplitude scaling by both the embedder and attacker. This differs from the analysis in [11] in that amplitude scaling is applied at both attacker and embedder, but as in practice embedding distortion is a small fraction of the original power in a channel this has little effect on the results.

The capacity results as the total capacity of the image (NC) obtained are shown in Table 2 along with the results from [6] for comparison purposes in Table 3. It should be noted that the analysis in [7] applies the NRCWT to 4 levels of decomposition rather than 3, but the low number of coefficients in the low pass level 3 NRCWT subband means that this will have little effect on the results. Also given are results for the NC-Spike model [11] where a 2 channel rather than 256 channel model is considered instead.

Figure 13. Lena EQ 256 parallel Gaussian channels for DTWT

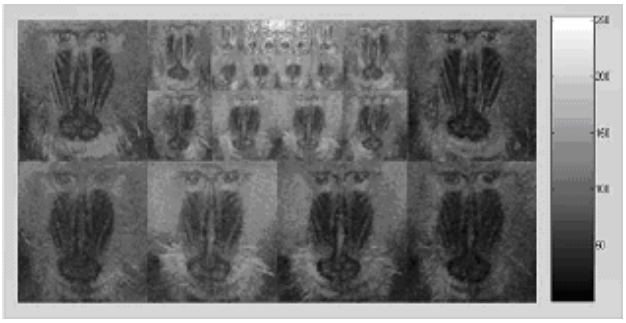

Figure 14. Baboon EQ 256 parallel Gaussian channels for DTWT

The subjective levels of distortion allocated to the embedder *D1* are the same as those employed in [11] and [6]. These are 10 for Lena and Peppers, 20 for Barbara, and 25 for Baboon. More textured images can tolerate more noise before the noise becomes visible. The attacker is then allowed to apply two different attack strengths *D2*. These are adjusted relative to the embedding distortion and are *2D1*, *5D1* and *10D1*.

The NRCWT produces the highest capacity estimates. This is a direct result of it producing more high power channels than the other wavelet transforms. The DTCWT produces the next highest capacity estimates as it still produces more high power channels than the DWT. This is due to the improved ability of these wavelet transforms to represent the host image in the wavelet domain. Higher power channels allow for greater robustness against the scaling introduced by the attacker and so higher per channel capacity. The Baboon image produces the highest capacity results, followed by the Peppers image and then the Barbara and Lena image. This can be explained by reference to the characteristics produced by the wavelet decompositions of these images. The large textured areas of the Baboon image produce a lot of large coefficients that lead to many high power and hence high capacity channels. By contrast the smoother images will have smaller coefficients and so fewer high power channels. It should be noted that a deficiency of this analysis is that it employs a simplification in that the host data is assumed to be uniform within each spread transform quantization cell. Essentially this is the equivalent of regarding the host power pk as being infinite in each channel; an assumption that leads to an under-estimation of the true performance of ST (spread spectrum) watermarking. This deficiency will be addressed in the next section.

TABLE II. TOTAL SPREAD TRANSFORM DATA HIDING CAPACITIES IN BITS FOR IMAGES OF SIZE 512X512

Image	D_1	$D_2 = 2D_1$		$D_2 = 5D_1$		$D_2 = 10D_1$	
		NC	NC-Spike	NC	NC-Spike	NC	NC-Spike
Lena (Daub-8 ST)	10	19486	17140	1877	3873	371	821
Lena (Bior.9/7 ST)		20333	17861	2057	4087	422	778
Lena (DTCWT ST)		26118	26717	2964	4698	565	997
Lena (NRCWT ST)		**37159**	**31216**	**5108**	**7596**	**1123**	**2317**
Baboon (Daub-8 ST)	25	48312	49858	7512	10970	1928	3333
Baboon (Bior.9/7 ST)		48583	50142	7692	11077	1968	3683
Baboon (DTCWT ST)		52231	53038	8023	11991	2576	4264
Baboon (NRCWT ST)		**60324**	**62513**	**11842**	**14953**	**3665**	**5485**
Peppers (Daub-8 ST)	10	27459	30064	2479	4574	391	700
Peppers (Bior.9/7 ST)		27338	29702	2621	4668	430	835
Peppers (DTCWT ST)		31934	35121	3095	5944	638	1211
Peppers (NRCWT ST)		**49523**	**51856**	**4374**	**7845**	**1606**	**3387**
Barbara (Daub-8 ST)	20	18943	27301	3677	5166	591	1301
Barbara (Bior.9/7 ST)		19486	27642	3651	4589	604	1282
Barbara (DTCWT ST)		22749	29737	4153	5432	811	1516
Barbara (NRCWT ST)		**37663**	**38538**	**5632**	**6934**	**1502**	**2593**

TABLE III. TOTAL DATA HIDING CAPACITIES IN BITS AS OBTAINED BY GHOUTI [6,7]

Image	D_1	$D_2 = 2D_1$		$D_2 = 5D_1$	
		NC	NC-Spike	NC	NC-Spike
Lena (Daub-8 ST)	10	27664	22080	3677	4818
Lena (Biorthogonal 9/7)		27233	21714	3651	4589
Lena (NRCWT)		**37512**	**30979**	**6061**	**6674**
Baboon (Daub-8)	25	26347	26148	4018	5455
Baboon (Biorthogonal 9/7)		24212	25218	3781	5842
Baboon (NRCWT)		**61394**	**57473**	**12555**	**11976**
Peppers (Daub-8)	10	19422	20708	3042	4344
Peppers (Biorthogonal 9/7)		16922	17852	2790	3962
Peppers (NRCWT)		**44004**	**33917**	**7127**	**6875**
Barbara (Daub-8)	20	22840	24495	3683	5475
Barbara (Biorthogonal 9/7)		18289	20026	2868	4531
Barbara (NRCWT)		**39045**	**37118**	**7041**	**8081**

3) Parallel Gaussian Channels

A deficiency of the analysis of the previous section is that it employs a simplification in that the host data is assumed to be uniform within each spread transform quantization cell. Essentially this is the equivalent of regarding the host power p as being infinite, an assumption that leads to an under-estatimation of the true performance of ST watermarking.

At low DWRs (document-to-watermark ratio) the embedding strength will overwhelm the host power and the probability that the host data will be quantised to anything other than the two centroids at the origin is negligible. In such cases performance can be improved by using very small values for the distortion compensation factor α.

This has the effect of dramatically increasing the size of the centroids at the origin and hence the robustness. As the host data will be gathered around the origin between the two possible centroids the accuracy of the embedding becomes much less important. The embedding strength needed to shift the host data to the appropriate quantization bin being very low. Effectively taking advantage of the low host power the algorithm begins to resemble a spread spectrum based one.

Perez-Freire at al. [14] term this distortion compensated spread spectrum, or DC-SS. It differs from classical SS schemes in that the strength of the watermark embedding is not fixed, but adjusted according to the distance to the nearest centroid.

They show that the effective SNR (signal-to-noise ratio) when employing such a scheme can be calculated as:

$$SNR_{DC-SS} = \frac{\xi\left(1-\lambda\alpha^2\right)}{1+\lambda\xi\left(1-\alpha\right)^2} \quad (34)$$

Where:

$$\varepsilon = 10^{(WNR/10)} \quad (35)$$

$$\lambda = 10^{(DWR/10)} \quad (36)$$

The optimum value of α for DC-SS can then be calculated as that which minimizes the probability of error:

$$\alpha_{DC-SS} = \frac{1+\xi+\lambda\xi-\left[\left(1+\xi+\lambda\xi\right)^2-4\lambda\xi^2\right]^{1/2}}{2\lambda\xi} \quad (37)$$

Finally the capacity of a DC-SS channel is calculated:

$$C_{DC-SS}\left(\lambda,\xi,\alpha\right) \cong \frac{1}{2}\log_2\left(1+SNR_{DC-SS}\right) \quad (38)$$

As shown in equation 20 the spreading factor r effects the WNR. It also has a corresponding effect on the DWR, effectively decreasing the DWR:

$$DWR_r = DWR_1 - 10\log_{10} r \quad (39)$$

At sufficiently low DWR DC-SS will offer improved levels of performance over that of standard ST embedding. Table 4 shows capacity estimates obtained taking into account the improved performance offered by DC-SS in the case of low DWR channels. The capacity increase tends to be relatively more significant for the DWT, as it will have more low power channels. However, the same trend of the NRCWT and the DTWT producing superior capacity estimates remains.

TABLE IV. TOTAL DATA HIDING CAPCITIES IN BITS AS OBTAINED BY GHOUTI [6,7]

Image	D_1	$D_2 = 2D_1$		$D_2 = 5D_1$	
		NC	NC-Spike	NC	NC-Spike
Lena (Daub-8 ST)	10	19486	17140	1877	3873
Lena (9/7 Linear phase filters ST)		20333	17861	2057	4087
Lena (DTCWT ST)		26118	26717	2964	4698
Lena (NRCWT)		**37159**	**31216**	**5108**	**7596**
Baboon (Daub-8)	25	48312	49858	7512	10970
Baboon (9/7 Linear phase filters)		48583	50142	7692	11077
Baboon (DTCWT)		52231	53038	8023	11991
Baboon (NRCWT)		**60324**	**62513**	**11842**	**14953**
Peppers (Daub-8)	10	27459	30064	2479	4574
Peppers (9/7 Linear phase filters)		27338	29702	2621	4668
Peppers (DTCWT)		31934	35121	3095	5944
Peppers (NRCWT)		**49523**	**51856**	**4374**	**7845**
Barbara (Daub-8)	20	18943	27301	3677	5166
Barbara (9/7 Linear phase filters)		19486	27642	3651	4589
Barbara (DTCWT)		22749	29737	4153	5432
Barbara (NRCWT)		**37663**	**38538**	**5632**	**6934**

3) Fixed Embedding Strategies

The problem with the distortion measure used is that unacceptably large local distortions can be globally compensated. The optimised embedding strategies take no account of the requirement for imperceptibility. For this reason in this section the JND models derived in section II are taken into account when applying the Gaussian watermarking game.

The embedder in the Gaussian watermarking game can take perceptual constraints into account by allocating embedding strength to channels based on a fixed embedding strategy. In addition to the two JND models described in section II, both PSC compliant watermarking

and even white embedding are taken into account.

1. Embedding energy allocated optimally as calculated in previous section.
2. Embedding energy allocated proportionally to JND profile derived by Chou's method.
3. Embedding energy allocated proportionally to JND profile derived by Loo's method.
4. Embedding energy allocated proportionally to host energy of channel.
5. Embedding energy allocated evenly across all channels.

The results for the different wavelet transforms are shown in figures 15-18. For relatively smooth images like Peppers and Lena Chou's JND is closer to the optimum embedding allocation. This is due to the ability of Chou's JND to more effectively isolate edges in the images. However for relatively textured images like Baboon and Barbara Loo's JND is closer to the optimal allocation. This is due to the weakness of Chou's JND when it comes to modelling textures, while due to being based on the wavelet coefficients; Loo's JND is able to take advantage of the coefficient's accurate modelling of textured regions.

It is also interesting to note that in the cases where Loo's JND performs better than Chou's JND the white embedding performs better than the PSC compliant embedding. This is due to the flatter host power distributions.

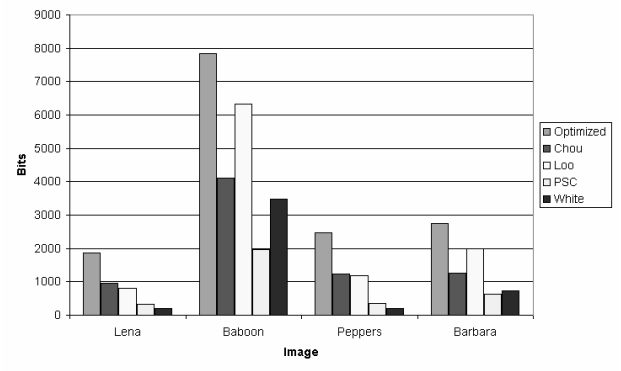

Figure 15. DWT (9/7 Linear phase filters) capacities for fixed embedding

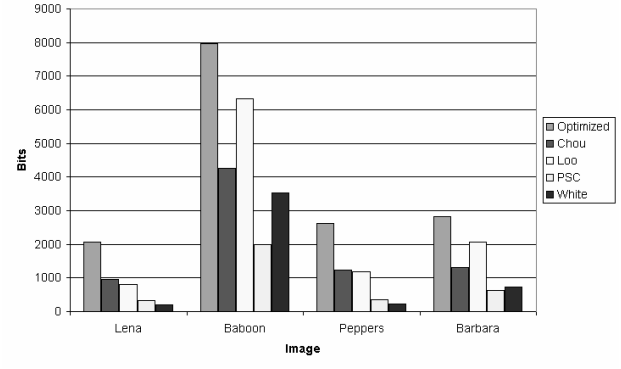

Figure 16. DWT (debauchies 8) capacities for fixed embedding

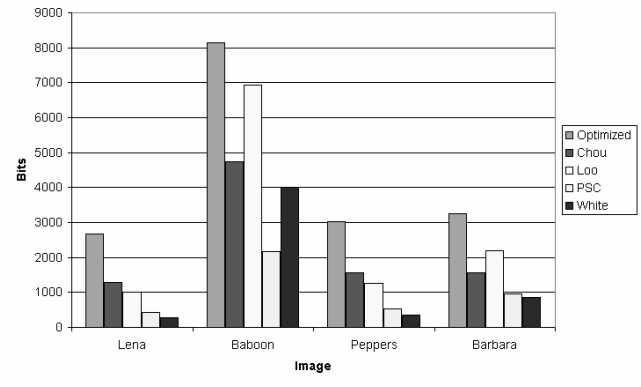

Figure 17. DTWT capcities for fixed embedding strategies

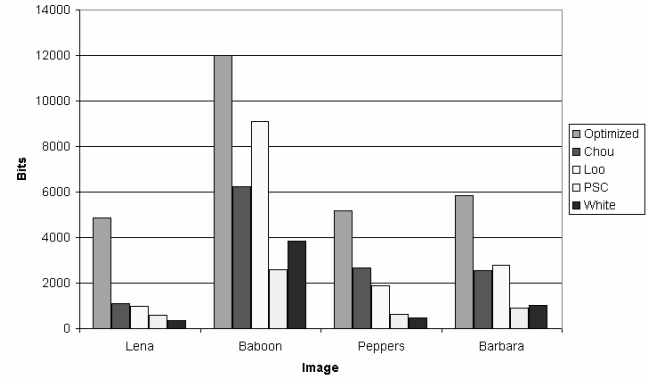

Figure 18. NRCWT capacities for fixed embedding strategies

For low details images like Peppers and Lena Chou's JND is closer to the optimum embedding allocation. This is due to the ability of Chou's JND to more effectively isolate edges in the images. However for higher detail images like Baboon and Barbara Loo's JND is closer to the optimal allocation. This is due to the weakness of Chou's JND when it comes to modelling textures, while due to being based on the wavelet coefficients, Loo's JND is able to take advantage of the coefficient's accurate modelling of textured regions.

It is also interesting to note that in the cases where Loo's JND performs better than Chou's JND the white embedding performs better than the PSC compliant embedding. This is due to the flatter host power distributions.

V. Experimental Results

Empirical bit error rates are given for a variety of different attacks and embedding scenarios.

Wiener filtering closely approximates the optimum attack distortion allocation and the results are as suggested by the capacity analysis with the NRCWT, DTWT and the DWT producing the best through worst results respectively.

Median filtering is less optimal as an attack but produces a comparatively larger distortion than Wiener filtering. The order of performance remains the same as the Wiener filtering case for all but the highest levels of distortion obtained when using the largest window size.

Mean filtering introduces the most severe distortion of the three low-pass filtering attacks introducing an unacceptable level of visual distortion even with the smallest window size. The NRCWT continues to produce the best results in the majority of cases.

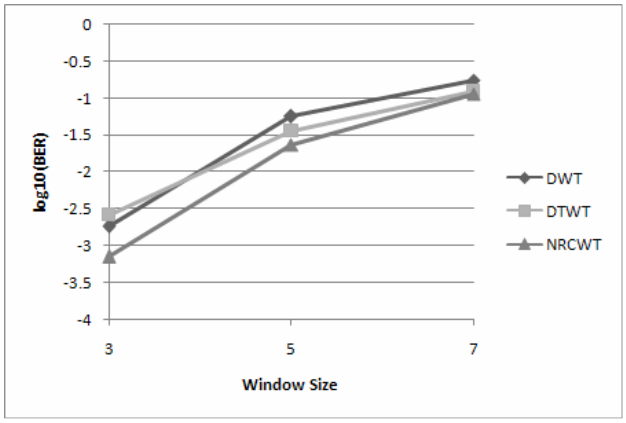

Figure 19. BERs for Wiener filtering attack applied for 512 bits embedded in 512x512 test images

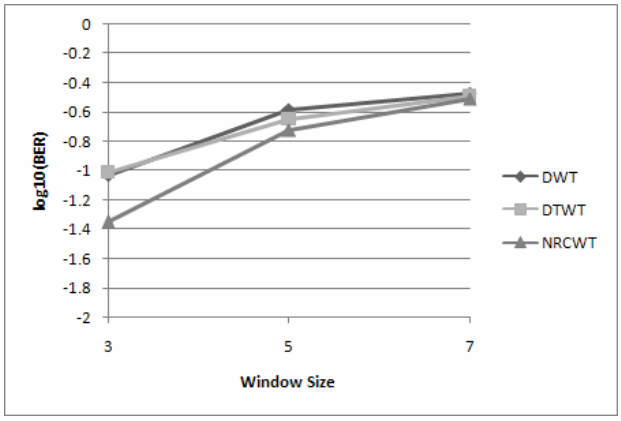

Figure 20. BERs for Median filtering attack applied for 512 bits embedded in 512x512 test images

The next attack considered is JPEG compression. Results are shown in figure 21. As JPEG compression is a weaker attack due to the perceptual shaping of the distortion, a longer watermark of length 1024 bits is used in the simulations for better clarity of results. The NRCWT again performs better than its counterparts; however the DWT in some cases performs better than the DTWT. This can be attributed to complications arising from the redundancy of the DTWT.

Results for AWGN attacks are shown in figure 22 for a watermark of length 1024 bits. The trend of the previous results is reversed in this case as the NRCWT produces the worst results with the DWT producing only slightly worse results than the DTWT.

The properties of the NRCWT that make it better at representing image features also causes the applied AWGN to create a bigger distortion in the NRCWT's wavelet coefficients. By contrast this effect is lessened in the DTWT and the DWT coefficients leading to better BER. While this would seem to contradict the capacity results obtained it should be noted that AWGN is a strongly sub-optimal attack as no scaling is applied. Due to the absence of scaling the greater magnitude of the NRCWT coefficients ceases to be an advantage. The DTWT produces slightly better results than the DWT in this case because of its superior ability to adapt to the image particularly at the higher frequency levels, this can be seen in the greater gap in performance for the highly textured Baboon image.

The distortion required for the AWGN attack to significantly decrease the performance is so large that it is unlikely an attacker would ever be able to apply such an attack without violating perceptual constraints. Low-pass filtering and JPEG compression are much more efficient means of attacking the embedded watermark as they simulate the scaling element of an optimal SAWGN attack, decreasing the performance of the watermarking system with a relatively much lower amount of distortion.

Results shown in figure 23 illustrate the effect of increasing the length of the watermark. As watermark length increases the size of the spreading vector and so the BER will increase as a result of the consequent lowering of the effective WNR with the probability of error almost disappearing completely when embedding only 512 bits.

For comparison with other watermarking algorithms the proposed system is also compared to spread transform complex wavelet algorithm proposed by Loo [9] and the spread spectrum DCT algorithm proposed by Bastug et al. [1]. Results are given for embedding in a 256x256 Lena image with 128 and 256 bits being embedded respectively. As can be seen from figures 24&25 the proposed algorithm performs well compared to others in the literature.

Also given are the ST algorithm's performance against scaling and cropping attacks in figures 26&27 respectively. The NRCWT continues to show the best performance when scaling is applied however all transforms show poor performance against the cropping attack. This is due to the multi-sample quantisation involved in spread transform watermarking and can be easily remedied through the use of simple repetition encoding.

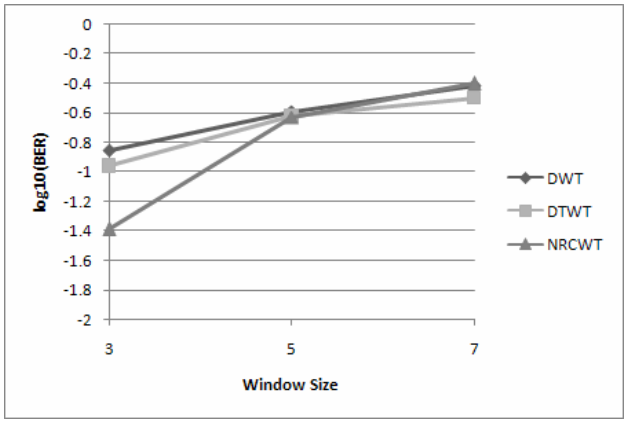

Figure 21. BERs for Mean filtering attack applied for 512 bits embedded in 512x512 test images

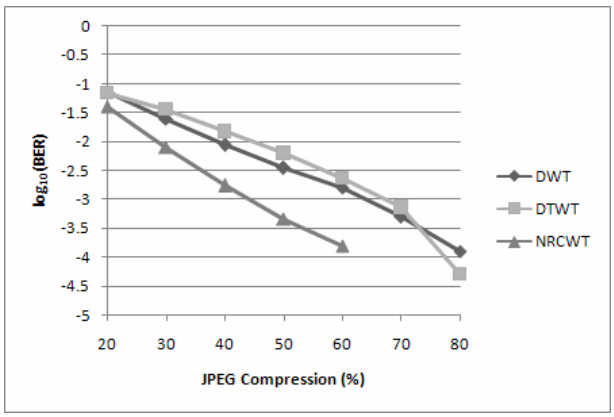

Figure 22. BERs for JPEG compression attack applied for 1024 bits embedded in 512x512 test images

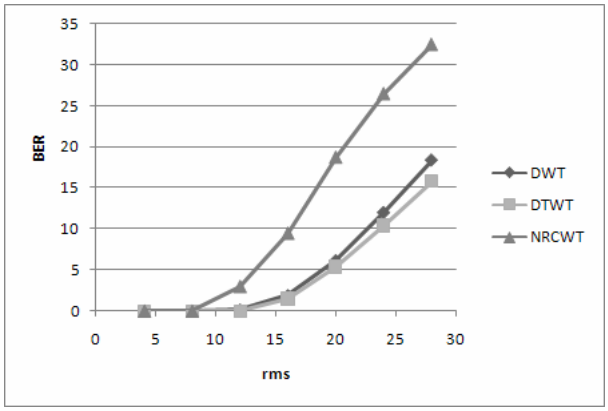

Figure 23. BERs for JPEG compression attack applied for 1024 bits embedded in 512x512 test images

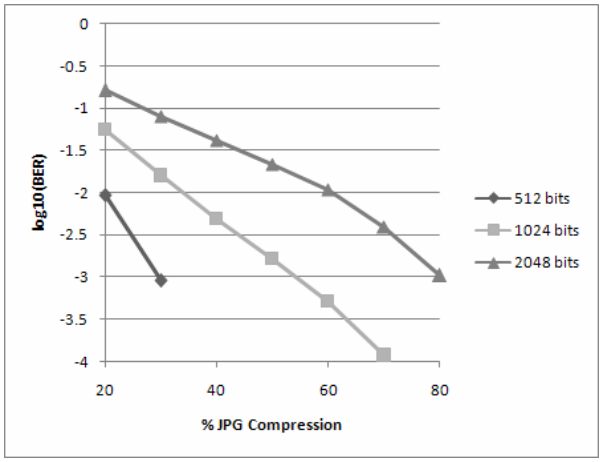

Figure 24. BERs for JPEG compression attack applied for 256 bits embedded in 256x256 Lena image

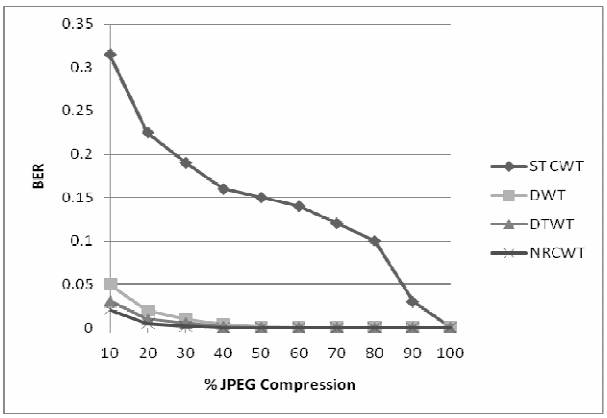

Figure 25. BERs for JPEG compression attack applied for 256 bits embedded in 256x256 Lena image

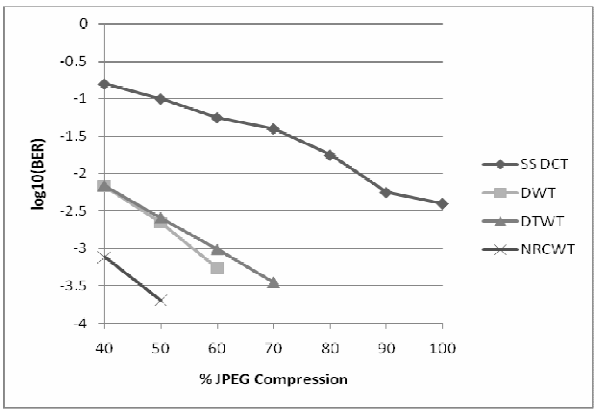

Figure 26. BERs for JPEG compression attack applied for 256 bits embedded in 256x256 Lena image

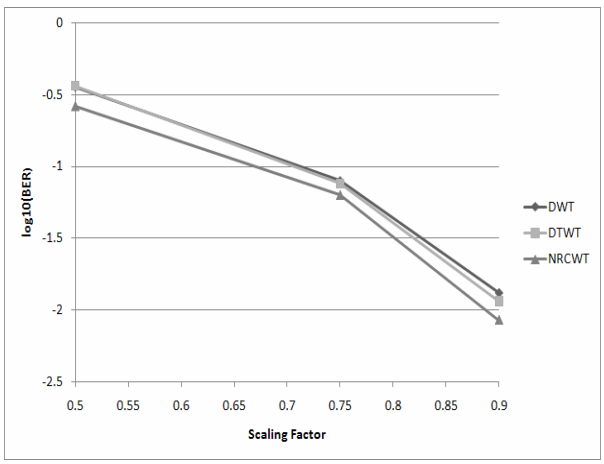

Figure 27. BERs for scaling factor attack applied for 512 bits embedded in 512x512 Lena image

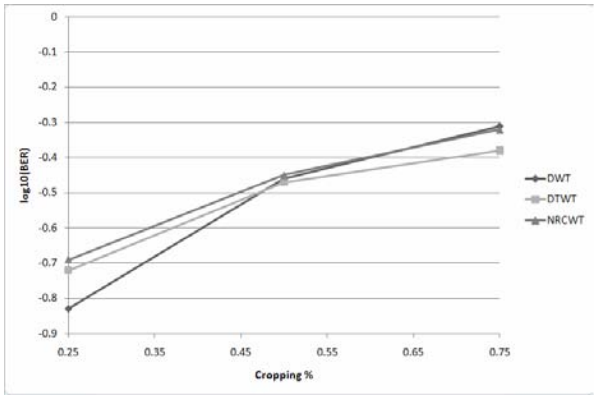

Figure 28. BERs for cropping % attack applied for 512 bits embedded in 512x512 images

VI. CONCLUSION

Then, two main methods of deriving a JND profile for the detailed wavelet transforms were presented. Chou's method offers the possibility of a universal JND model that can be applied to any watermarking scenario regardless of the transform being used. It is also very good at adapting watermark to signals to fine image features. However it shows weakness with regards to modelling complex textures within images.

Loo's model compensates for this by taking advantage of the excellent texture representation provided by wavelet transforms. However exhaustive visual tests must be conducted for each wavelet transform used. In addition Loo's model can lead to a spreading of the watermark signal around fine image features such as edges. In order to combine the advantages of both, a hybrid model is proposed and used.

By applying the principles of spread transform embedding the benefits of both quantization and spread spectrum are combined in the proposed system. This chapter has demonstrated both theoretically and empirically the improved levels of performance offered by the DTWT and NRCWT combined with the high capacities offered by spread transform embedding. This is due to the higher power channels offered by the NRCWT and DTWT due to their superior ability to represent the features of the host image. Further, the analysis clearly shows the areas of the image such as textured and low frequency components, into which watermarks should be embedded to maximise the capacity.

Further, the case of non-iid data was considered as well as the application of fixed embedding strategies to the theoretical analysis. This analysis shows the validity of combining both Chou and Loo's JND models to create a balance between adaptability in both simple and complex images.

Experimental results back up these findings and the obtained capacity results, taking into consideration several common attacks such as low-pass filtering, JPEG compression and Gaussian noise.

REFERENCES

[1] A. Bastug and B. Sankur, "Improving the payload of watermarking channels via ldpc coding," IEEE Signal Processing Letters, vol. 11, pp. 90-92, February 2004.

[2] B. Chen, G. Wornell, "Quantization Index Modulation: A Class of Provably Good Methods for Digital Watermarking and Information Embedding", IEEE Trans. Inform. Theory, Vol. 47, No. 4, May 2001.

[3] C. H. Chou and Y. C. Li, "A perceptually tuned subband image coder based on the measure of just-noticeable-distortion profile" IEEE Trans. Circuits and Systems for Video Technol,, Vol. 5, pp. 467-476, December 1995.

[4] Joachin Eggers and Bernd Girod, "Informed Watermarking", Kluwer Academic Publishers, May 2003, ISBN 1402070713.

[5] Felix C. A. Fernandes, Michael B. Wakin and Richard G. Baraniuk, "Non-redundant, linear phase, semi-orthogonal, directional complex wavelets", In Proc. Int. Conf. on Acoustics, Speech and Signal Processing (ICASSP). Montreal, Quebec, Canada, 2004.

[6] L. Ghouti, A. Bouridane, M. K. Ibrahim, S. Boussakta, "Digital image watermarking using balanced multiwavelets", *IEEE* Transactions on Signal Processing, Vol. 54, No. 4, April 2006.

[7] L. Gouti, "Data-Hiding Capacities of Non-Redundant Complex Wavelets", IET Int. conference on Visual Information Engineering (VIE2006), Bangalore, India, 26-28 Dec. 2006.

[8] N. Kingsbury, "The dual tree complex wavelet transform: A new efficient tool for image restoration and enhancement", Proc. EUSIPCO 98, pp. 319-322, Rhodes, Greece, Sep. 1998.

[9] P. Loo, "Digital Watermarking using Complex Wavelets". PhD thesis, University of Cambridge, March 2002.

[10] S. M. Lopresto, K. Rachandran, and M. T. Orchard. "Image coding based on mixture modeling of wavelet coefficients and a fast estimation-quantization framework". In Proc. DCC'97 (IEEE Data Compression Conference), Snowbird, Utah, USA, March 1997.

[11] P. Moulin. "The role of information theory in watermarking and its application to image watermarking". Signal Processing, Special Issue on Information-Theoretic Issues in Digital Watermarking, Vol. 81 No. 6, June 2001.

[12] P. Moulin and M. C. Mihcak, "The parallel-gaussian watermarking game", IEEE Trans. Inform. Theory, Vol. 50, pp. 272-289, February 2004.

[13] N. Nikolaidis, I. Pitas, "Robust Image Watermarking in the Spatial Domain", Signal Processing, Vol. 66 , Issue 3 (May 1998), pp. 385 – 403, 1998.

[14] L. Perez-Freire, F. Perez-Gonzalez and S. Voloshynovskiy, "An Accurate Analysis of Scalar Quantization-Based Data Hiding", IEEE Transactions on Information Forensics and Security, Vol. 1, No. 1, March 2006.

[15] I. W. Selesnick, “The double density dual tree DWT”, Trans. On Signal Processing, Vol. 52 No. 5, pp.1304-1314, May 2004.

[16] A. I. Thompson, A. Bouridane, F. Kurugollu, “Spread Transform Capacities for Image Media Using Complex Wavelets”, International Symposium on Signal Processing and its Applications 2007 (ISSPA 2007), 12 - 15 February 2007, Sharjah, United Arab Emirates (U.A.E.).

[17] A. I. Thompson, A. Bouridane, F. Kurugollu, “Spread Transform Watermarking for Digital Multimedia Using the Complex Wavelet Domain”, The 2007 ECIS Symposium on Bio-Inspired, Learning, and Intelligent Systems for Security (BLISS 2007), August 9-10, 2007, Edinburgh, UK.